Identifying Regions of Oscillations and Describing the Behaviour of a Simple Model for Cool Flames, Sal'nikov's Reaction, P → A → B, Occurring in a Spherical Batch Reactor with Varying Degrees Natural Convection

A. N. Campbell*, S. S. S. Cardoso* and A. N. Hayhurst

Department of Chemical Engineering, University of Cambridge, Pembroke Street, Cambridge CB2 3RA, UK.

* Corresponding Author. Tel. +44 1223 334777; Fax. +44 1223 334796;

E-mail addresses: anc31@cam.ac.uk, sssc1@cam.ac.uk

Abstract

When cool flames, or indeed any exothermic chemical reaction, occur inside an unstirred vessel, the heating effect of the reaction often induces temperature gradients and consequently natural convection. The intensity of the resulting flow is governed by the Rayleigh number (*Ra*). This work examines the behaviour of Sal'nikov's reaction, which is the simplest reaction to exhibit the thermokinetic oscillations that characterise cool flames, under the influence of natural convection in an unstirred spherical reactor, by means of numerical simulation. A region on a regime diagram in which oscillations are observed has been sought for fixed values of the first-order rate constants for Sal'nikov's reaction. The region found could be split into two distinct areas, one for $Ra < 10^3$, where diffusion dominates transport, and one when $10^3 < Ra < 10^6$, when laminar convection dominates. There is a distinct change in shape of the region of oscillations around the critical value of $Ra \sim 10^3$, when natural convection becomes important. When diffusion dominated transport, the boundaries between oscillatory and non-oscillatory solutions are largely independent of the ratio of timescales, $\tau_{step\ 2} / \tau_{convection}$, and agreed well with the values found previously in the purely diffusive limit. When natural convection was important, the oscillations occurred over a wider range of parameters, and the width of the oscillatory region increased with *Ra*.

In addition to defining a region of oscillations, the different types of behaviour in different parts of the regime diagram are discussed. In general, it was found that the inclusion of natural convection led to a number of different types of behaviour, which were far more complex than those seen in the absence of natural convection. The non-oscillatory cases, with relatively small increases in temperature, had similar temporal evolutions of the temperature and the concentration of A at the centre of the reactor regardless of the degree of convection present. It was also shown that in this region of slow reaction, the concentration of A remained virtually spatially uniform at Rayleigh numbers sufficient to generate significant natural convection. This is similar to the diffusive case. Natural convection did, however, have an impact on the shape of the temperature profile along the vertical axis of the reactor. Finally, for the non-oscillatory,

high temperature rise solutions with natural convection, the forms of the solutions were found to be initially very similar to those seen in the purely diffusive limit, due to the relatively large induction time for flow due to natural convection.

Nomenclature

a	concentration of the intermediate A
C_P	specific heat at constant pressure
C_V	specific heat at constant volume
D_A	diffusion coefficient of the intermediate A
E_i	activation energy of step i of Sal'nikov's reaction
g	acceleration due to gravity
k_i	rate constant of step i of Sal'nikov's reaction
$k_{2,0}$	rate constant of step 2 evaluated at $T = T_0$
L	characteristic length (radius) of the reactor
Le	Lewis number, $Le = \kappa / D_A$
p	concentration of precursor P
p_0	initial concentration of P
$\mathscr{P}$	pressure
$\mathscr{P}_0$	initial pressure
Pr	Prandtl number, $Pr = \nu / \kappa$
q_i	exothermicity of step i of Sal'nikov's reaction
R	universal gas constant
Ra	Rayleigh number, $Ra = \beta g L^3 \Delta T / \kappa \nu$
t	time
$\underline{u}$	velocity
U	characteristic velocity
T	temperature
T_0	constant wall temperature
x	horizontal coordinate, measured from the centre of the reactor
y	vertical coordinate, measured from the very bottom of the reactor on the vertical axis
Z_2	pre-exponential factor in Arrhenius expression for k_2

Greek

β	coefficient of thermal expansion
γ	ratio of principal specific heats
ΔT	characteristic temperature increase
κ	thermal diffusivity
ν	kinematic viscosity
ρ	density
ρ_0	density at $T = T_0$
$\tau_{convection}$	timescale for convection
$\tau_{diffusion}$	timescale for diffusion of heat
τ_i	induction period for natural convection
$\tau_{step\ i}$	timescale for step *i* of Sal'nikov's reaction

1. Introduction

Oscillatory cool flames, which are a feature of the low-temperature combustion of a hydrocarbon, have received an increasing amount of attention in recent years. These cool flames occur at the transition from slow combustion to ignition and arise due to the complex interaction of thermal and chemical feedback and heat loss to the surroundings [1, 2]. When any exothermic reaction, such as cool flames, occurs in a fluid within a closed vessel, spatial temperature gradients are induced. If these gradients become sufficiently large, the resulting buoyancy forces will cause the gas to move. This natural convection can have a significant influence on the progress of the reaction. The nature of the induced flow is determined by the Rayleigh number, $Ra = (\beta g L^3 \Delta T) / (\kappa \nu)$. Natural convection becomes significant when Ra increases above a threshold value of $\approx 10^3$ [3]. Most experimental measurements on cool flames have, however, been made in unstirred vessels, so the effects of buoyancy have not been accounted for [4]. The significant effect that natural convection has on the development of the temperature field within a reactor during a cool flame has been shown by interferometry [5, 6]. Despite the interesting, and highly significant behaviour observed in these studies, very little experimental, numerical

or theoretical work has been carried out to try and elucidate the effects of the interaction of the complex chemical phenomena and the flow due to natural convection.

Recently, the striking effects of natural convection on the development of cool flames has been shown by a series of experiments carried out by Pearlman and co-workers [7 – 9], who studied *n*-butane/oxygen cool flames in a 500 cm^3 spherical, unstirred vessel at both terrestrial conditions and in microgravity, which was achieved aboard the NASA KC-135 aircraft executing a parabolic flight plan. The results showed that in microgravity, *i.e.* in the absence of natural convection when diffusion would be the only significant means of heat and mass transfer, the cool flames initiated at the centre of the reactor, where the temperature would be at its maximum within the vessel, and then propagated outwards with radial symmetry. In stark contrast to this, at terrestrial conditions the flame initiates at the top of the vessel and propagates vertically downwards in a horizontal flame front.

In addition to this experimental work, there have been some theoretical and numerical studies of the effects of natural convection on a simplified model of cool flames, namely Sal'nikov's reaction [10], which is the simplest scheme to exhibit the thermokinetic oscillations that characterise cool flames. The reaction consists of two consecutive first-order steps:

$$\mathrm{P} \xrightarrow{1} \mathrm{A} \xrightarrow{2} \mathrm{B}\,, \qquad \text{(I)}$$

where a precursor P is converted to a product B, *via* an active intermediate A. The first step is assumed to be thermoneutral, with E_1, its activation energy, and q_1, the exothermicity of step 1, both equal to zero. Step 2 is considered to be exothermic, with $E_2 > 0$ and $q_2 > 0$. This mechanism is of course a considerable simplification of that which governs cool flames, which includes chemical feedback through chain branching in addition to the purely thermal feedback present in Sal'nikov's reaction. Nevertheless, Sal'nikov's reaction has often been used to represent cool flames and does yield significant insight into the interaction of thermokinetic oscillations and natural convection. Sal'nikov's reaction has been extensively studied in the limit of perfect mixing [11 – 15] where diffusion and convection can be ignored. These studies defined, by means of a stability analysis, a region of parameter space in which oscillations in the temperature and in the concentration of the intermediate A occur. Work has also been

carried out on another limiting case, where the transport of heat and mass is purely diffusive [16]. This diffusive limit corresponds to reaction occurring in microgravity, as studied experimentally [7 – 9] and numerically [17, 18]. More recently, numerical studies have investigated the influence of natural convection on Sal'nikov's reaction. Cardoso *et al.* [19] reported some preliminary results on the development of natural convection in a spherical vessel containing a gas undergoing Sal'nikov's reaction.

A more detailed investigation of the development of convection [20] showed through appropriate scaling of the governing equations that the behaviour of this system depends on three non-dimensional groups, each of which can be expressed as the ratio of the timescales of two of the three interacting phenomena, namely chemical reaction, diffusion and convection. A system undergoing Sal'nikov's reaction can therefore be represented as a point on the three-dimensional (3-D) diagram in Fig. 1. The axes of this diagram correspond to each non-dimensional group. The horizontal plane in this diagram, described by the axes $\tau_{step\ 2} / \tau_{convection}$ and $(\tau_{step\ 2} / \tau_{step\ 1})\ p'$, where p' is the dimensionless concentration of the precursor P, corresponds to the well-mixed case, whereas the vertical plane defined by the axes $\tau_{step\ 2} / \tau_{diffusion}$ and $(\tau_{step\ 2} / \tau_{step\ 1})\ p'$ corresponds to the purely diffusive case. In a general Sal'nikov system (point C in Fig. 1), both diffusion and natural convection will play a role. A straight line through the origin of the plane described by the axes $\tau_{step\ 2} / \tau_{convection}$ and $\tau_{step\ 2} / \tau_{diffusion}$ (for any fixed $(\tau_{step\ 2} / \tau_{step\ 1})\ p'$) represents a constant value of the Rayleigh number.

This analysis was extended by Campbell *et al.* [21, 22] who studied the behaviour of this reaction in a spherical reactor both in the presence and absence of natural convection and found oscillations in the temperature and the concentration of A over a range of parameters. One interesting aspect of these oscillations was examined further [23]; it was found that when the ratio $\tau_{step\ 2} / \tau_{convection}$ increases beyond ~ 15, the oscillations in the temperature and the concentration of the intermediate A are in-phase in certain parts of the reactor. This is in contrast to the behaviour seen in the well-mixed and purely diffusive limits, where only approximately anti-phase oscillations were observed.

As of yet, however, no effort has been made to identify a region on the regime diagram in Fig. 1 in which oscillations are observed when convection is present to some degree. Previously, a region of oscillations has been identified numerically for the purely

diffusive case [24]. This work therefore aims to identify a region in parameter space where thermokinetic oscillations are observed, by means of numerical simulation, and to characterise the different types of behaviours seen in different regions of the regime diagram.

2. Governing Equations

For the purposes of this work, the modelling approach first proposed by Cardoso *et al.* [20] is considered. The governing equations express the conservation of the reactants, energy, momentum and mass. The adoption of the Boussinesq approximation, in which density changes are ignored, except insofar as they give rise to a buoyancy force, considerably simplifies the governing equations; the conditions under which such a simplification is valid are discussed below. This approach has been adopted and extended by others [8] in the modelling of cool flames. Recently, a comparison of this modelling approach and experimental measurements of the temperature for a simpler, one-step exothermic reaction occurring in a spherical batch reactor was performed [25]. It was found that analytical scaling expressions and numerical simulations both agreed very well with measured temperatures at the centre of the reactor, and that the shape of the temperature profile along the vertical axis of the reactor generated numerically agreed very well with that found experimentally over a wide range of *Ra*. This numerical study, combined with previous experimental work [26, 27] showed that for a spherical reactor, natural convection becomes important when *Ra* rises above ~ 500.

The equation governing the conservation of the active intermediate A can be written as:

$$\frac{\partial a}{\partial t} + \underline{u}.\nabla a = D_A \nabla^2 a + k_1 p_0 \exp(-k_1 t) - k_2(T) a \,, \qquad (1)$$

where a is the concentration of species A, D_A is its molecular diffusivity $\underline{u}$ is the velocity vector k_1 is the first-order rate constant for step 1 of reaction (I) and k_2 is the first-order rate constant of step 2. It is assumed in this equation that the concentration of P in the reactor is initially uniform ($p = p_0$), and that it remains so, equal to $p_0 \exp(-k_1 t)$,

throughout the course of the reaction. This assumption depends on k_1 being independent of temperature (because $E_1 = 0$) and holds only for relatively small increases in temperature.

Conservation of energy is written as:

$$\frac{C_V}{C_P}\frac{\partial T}{\partial t} + \underline{u}.\nabla T = \kappa\nabla^2 T + \frac{q_2 k_2(T)}{\rho_0 C_P} a\,, \tag{2}$$

where κ is the thermal diffusivity and ρ_0 is the density at the initial temperature T_0. Conservation of momentum is given by the Navier-Stokes equations. As mentioned above, these equations can be simplified by adopting the Boussinesq approximation. It is shown below that usually $\Delta T << T_0$, and hence the Boussinesq approximation is appropriate; this also justifies the form of the generation term in Eq. (1), because the assumption that P remains spatially uniform throughout depends on there being no significant change in temperature or density inside the reactor. In the buoyancy term the variation of density is described by

$$\rho = \rho_0\left[1 - \beta(T - T_0)\right], \tag{3}$$

The Navier-Stokes equations therefore become:

$$\frac{\partial \underline{u}}{\partial t} + \underline{u}.\nabla\underline{u} = -\frac{1}{\rho_0}\nabla\left(\mathscr{P} - \mathscr{P}_0\right) + \nu\nabla^2\underline{u} + \frac{\rho - \rho_0}{\rho_0}\underline{g}\,. \tag{4}$$

The final equation required is the continuity equation, which can be expressed in its incompressible form due to the adoption of the Boussinesq approximation,

$$\nabla.\underline{u} = 0\,. \tag{5}$$

Initially, the gas in the reactor is considered to be pure P, at temperature T_0. There is no initial motion in the gas. Throughout the reaction, the temperature of the wall is held constant at T_0. This, of course, means that heat can be removed from the system at the wall. It is also assumed that the no-slip condition holds at the wall, and that there is no flux of any species at the wall. The effects of surface chemistry are therefore neglected. The initial and boundary conditions can thus be stated:

$$t = 0: \quad p = p_0;\ \ a = 0;\ \ T = T_0;\ \ \underline{u} = 0 \ \ \forall\underline{x}$$

$$\text{At the wall}: \quad \underline{n}.\nabla p = \underline{n}.\nabla a = 0;\ \ T = T_0;\ \ \underline{u} = 0\,, \tag{6}$$

where $\underline{n}$ is the unit vector normal to the surface.

The axes in Fig. 1 are defined as the ratios of the characteristic timescales for reaction, diffusion of heat (which can be related to diffusion of mass *via* the Lewis number) and natural convection. These are defined as:

$$\tau_{step\ 1} = \frac{1}{k_1};\ \ \tau_{step\ 2} = \frac{1}{k_{2,0}};\ \ \tau_{diffusion} = \frac{L^2}{\kappa};\ \ \tau_{convection} = \frac{L}{U}, \tag{7}$$

where $k_{2,0}$ is the rate constant for step 2 of reaction (I) evaluated at T_0. The characteristic velocity due to natural convection, U, takes the form suggested by Campbell *et al.* [21, 22], *i.e.*

$$U \sim \left(\beta g L^3 \Delta T\right)^{1/2}, \tag{8}$$

where the characteristic temperature rise ΔT is given by

$$\Delta T \sim \left(\frac{q_2}{C_P}\right)^{2/3}\left(\frac{k_1^2 L}{\beta g}\right)^{1/3}. \tag{9}$$

3. Numerical Method

Equations (1) – (6) were solved numerically for a spherical batch reactor using the PDE solver *Fastflo* [28]. The algorithm employed utilises the finite element method and is the same as that outlined elsewhere [20]. For the purposes of the numerical simulations, the thermal decomposition of di-*t*-butyl peroxide was considered, because this has been shown to behave like Sal'nikov's reaction under certain conditions [29, 30]. In these studies, the thermal decomposition of di-*t*-butyl peroxide represented step 2 of Sal'nikov's reaction, with the thermoneutral first step being mimicked by the slow admission of the reactant into a well-mixed reactor. The following parameters were chosen to match those used in previous numerical studies [19 – 25]. The temperature of the wall of the spherical reactor was held constant at T_0 = 500 K and the physicochemical properties used were as follows: the initial molar density ρ_0 = 8.2 mol m^{-3} (corresponding to a pressure of 0.34 bar at 500 K), the heat capacity at constant volume C_V = 190 J mol^{-1} K^{-1}, and the exothermicity of step 2, q_2 = 400 kJ mol^{-1}. The chemistry is defined such that the rate constant k_1 = 0.025 s^{-1}, corresponding to $\tau_{step\ 1}$ = 40 s, and $k_2 = Z_2 \exp(-E_2 / RT)$

with $Z_2 = 2 \times 10^{15}$ s^{-1} and $E_2 = 152$ kJ mol^{-1}. These values give $k_2 = k_{2,0} = 0.265$ s^{-1} at 500 K, and $\tau_{step\ 2} \sim 4$ s, *i.e.*, step 2 is an order of magnitude faster than step 1 in reaction (I). In the present work, the effect of altering the values of these rate parameters is not considered. Furthermore, the simplifying assumption that both the Lewis and Prandtl numbers were unity was made. This implies that $\nu = \kappa = D_A$, *i.e.*, the diffusivities of momentum, heat and chemical species were considered to be equal. Different regions of the regime diagram in Fig. 1 were explored by varying the radius of the reactor, L, over the range 0.01 – 0.15 m, the acceleration due to gravity, g, over the range 0.1 – 3000 m s^{-2} and the diffusivity κ over the range 3×10^{-6} – 1.4×10^{-3} m^2 s^{-1}.

4. Defining a Region of Temporal Oscillations

A region in the regime diagram in Fig. 1 in which oscillations occur under the influence of natural convection is to be found. Consider a system with reaction, diffusion and convection; this system is represented as a point (C) in the general 3-D regime diagram shown in Fig. 1. As reaction progresses, p' decreases and hence the working point, locating the system on the diagram, moves along a line parallel to the ($\tau_{step\ 2}$ / $\tau_{step\ 1}$) p' axis. However, if step 1 is much slower than step 2, p' decreases slowly and the pool chemical approximation is valid. Thus, it may be assumed that p' is approximately constant. Under these conditions the working point does not move in the 3-D diagram. This is true in general for step 1 of Sal'nikov's reaction being very slow. For the specific case considered in this work, *i.e.* with the precursor P being initially uniformly distributed throughout the reactor and remaining thus as the reaction proceeds, a similar analysis to that performed for the purely diffusive regime [24] can be performed, thereby showing that p' is in fact a function of the ratios of timescales that appear on the other axes. In this case, p' can be removed from the axis of the regime diagram. Attention can therefore be focused on the 2-D plane, defined by the $\tau_{step\ 2}$ / $\tau_{diffusion}$ and $\tau_{step\ 2}$ / $\tau_{convection}$ axes (for a constant value of $\tau_{step\ 2}$ / $\tau_{step\ 1}$), containing the working point. It was shown by Campbell *et al.* [24] that in the diffusive limit, oscillations occurred over a finite range of $\tau_{step\ 2}$ / $\tau_{diffusion}$. The $\tau_{step\ 2}$ / $\tau_{diffusion}$ axis of the 2-D regime diagram corresponds to the diffusive

limit, so this finite range of oscillations should be defined on this axis. Similarly, a closed region of parameter space in which oscillations occur for the well-mixed case was identified by Gray and Scott [13]. The well-mixed limit corresponds to the $\tau_{step\ 2}$ / $\tau_{convection}$ axis of the 2-D diagram. This oscillatory region could be mapped onto the axis of the regime diagram in Fig. 1. It seems logical to conclude, therefore, that the region of oscillations when natural convection plays a role would join these two limiting cases.

The region of oscillations was defined by carrying out a series of many simulations. It should be noted that these simulations were for $Ra < 10^6$. Only the region of oscillations in the presence of weak and laminar natural convection is therefore considered.

The results of these simulations are shown on the 2-D regime diagram in Fig. 2. The Rayleigh number was calculated using the expression:

$$Ra = 5.40 \frac{\left(\tau_{step\ 2} / \tau_{convection}\right)^2}{\left(\tau_{step\ 2} / \tau_{diffusion}\right)^2}, \qquad (10)$$

where the numerical factor (from [21, 22]) ensures that the Rayleigh numbers calculated in this manner are similar to those observed in the simulations.

The region in which oscillations were observed is shaded. If this region of oscillations is considered, it is clear that there are two distinct sections, namely that when $Ra < 10^3$, when diffusion is still dominant, and when $Ra > 10^3$ and natural convection becomes much more significant. When $Ra < 10^3$, the boundaries between the non-oscillatory and oscillatory solutions remain at an approximately constant value of $\tau_{step\ 2}$ / $\tau_{diffusion}$ for increasing $\tau_{step\ 2}$ / $\tau_{convection}$. These boundaries in the region of oscillations are in good agreement with the results for a purely diffusive system [24]. When *Ra* reaches ~ 10^3, there is a sharp change in the shape of the region of oscillations. This change is obviously due to natural convection superceding diffusion as the dominant transport mechanism. The fact that this change is observed at a Rayleigh number of just below 10^3 provides further confirmation that the model being used in the numerical simulations is capturing the principal physical processes correctly. Previous experimental [26, 27] and numerical [25] studies showed that natural convection becomes significant when *Ra* is just below 10^3. When *Ra* exceeds 10^3, the shape of the oscillatory region is dramatically different. It is evident that oscillations occur over a very wide range of $\tau_{step\ 2}$ / $\tau_{convection}$. It

is interesting to note that as *Ra* increases, the region of oscillations defined in Fig. 2, increases significantly in size. As alluded to previously, the turbulent regime has not been considered in the present work. Obviously, as natural convection becomes turbulent, the degree of mixing in the reactor will increase. This will significantly affect the behaviour of the system. It would be interesting to see if there is a sharp change in the shape of the oscillatory region at the transition to turbulence, similar to that seen in Fig. 2 at the transition from weak or no flow, to laminar convection. The region of oscillations defined in Fig. 2 is, of course, for a fixed value of $\tau_{step\ 2} / \tau_{step\ 1}$, so in fact only represents a cross-section of a general 3-D space in which oscillations occur. A map of this 3-D space could be built up by performing simulations at different values of $\tau_{step\ 2} / \tau_{step\ 1}$; however, there is no reason to believe that the general shape of the 2-D cross-sections would be any different. The boundaries of the system on the axes, represented by regions of stability in the purely diffusive and well-mixed limits, would change according to the value of $\tau_{step\ 2} / \tau_{step\ 1}$, but it seems likely that the region joining these two limiting cases, *i.e.* the region in which natural convection is significant, would be of similar shape to that seen in Fig. 2.

As one might expect, the oscillatory behaviour seen within the region defined in Fig. 2 is not consistently identical throughout the different areas of the diagram. Various types of behaviour are seen, depending on the location in the regime diagram. The different types of behaviour observed are discussed in the next section, and in addition, the non-oscillatory regions are also examined.

5. Identifying Different Regions of Behaviour

5.1 Numerical Results

Fig. 3 shows the development of the temperature and the concentration of A in a vertical cross-section through the centre of the reactor as time progresses, for the five cases highlighted on Fig. 2. Details of these five cases appear in Table 1. Each case is characteristic of a different region of behaviour in the regime diagram; these will be discussed in turn.

Case A is typical of a region of sustained oscillations seen when diffusion is still dominant ($Ra < 10^3$). The behaviour in this part of the regime diagram is very similar to that seen in the purely diffusive case, with anti-phase oscillations in the temperature and the concentration of A evident. The weak natural convection that is present causes a distortion of the spherical symmetry seen in purely diffusive system, with the maximum temperature occurring above the centre of the reactor. At values of $\tau_{step\ 2} / \tau_{diffusion} > 2$, *i.e.* above the region of oscillations in Fig. 2, the solutions of the governing equations are very similar to the non-oscillatory, low temperature rise solutions observed in the purely diffusive limit [24]. In this case the temperature within the vessel rises slowly to its maximum, which is considerably lower than the maximum seen in case A. The concentration of A also increases slowly and remains approximately spatially uniform throughout. The non-oscillatory solutions with $\tau_{step\ 2} / \tau_{diffusion} < 0.5$ are similar in form to the high temperature rise solutions described previously [24]. There is an initial rise in the concentration of A, which then falls very rapidly to approximately zero throughout the reactor. This is accompanied by a much larger rise in the temperature. As with case A, the only difference between the behaviour seen in the non-oscillatory cases with $Ra < 10^3$ and the purely diffusive (*i.e.* $Ra = 0$) cases is the slight distortion of the temperature field within the reactor.

When Ra increases above 10^3, there are further interesting regions of behaviour. Case B is in a similar area of the regime diagram to the non-oscillatory, high temperature rise solutions, discussed above; however, the Rayleigh number is higher ($\sim 10^4$), thus convection is having a significant influence on the progress of the reaction. It is interesting to note that the temperature and concentration fields shown for case B in Fig. 3 at small times ($< \sim 3$ s) are almost symmetric; however, this symmetry is disrupted by the natural convection which does develop at larger times. It can be seen that for $t > 3$ s, the temperature profile becomes more skewed, with the hot zone moving upwards in the reactor. Eventually, a degree of stratification in the temperature is evident, as would be expected in a system where natural convection is important. As was the case in the non-oscillatory, high temperature rise regime in the purely diffusive limit, the temperature rises are considerably larger than those seen in the oscillatory region in Fig. 2, and after

an initial increase in the concentration of A, it falls to virtually zero throughout the reactor except within a thin layer at the wall.

When $\tau_{step\ 2} / \tau_{convection}$ increases, the system moves into the region where oscillations are observed. When natural convection is significant, the oscillatory behaviour is more complex, and there is a notable difference between this and the behaviour seen in the purely diffusive case. Case C is typical of the oscillatory behaviour seen in the region on the regime diagram defined by $\tau_{step\ 2} / \tau_{diffusion} < 0.5$ and $5 < \tau_{step\ 2} / \tau_{convection} < 15$. In contrast to case B, it is evident from Fig. 3 that natural convection is significant throughout the time period considered. The hot zone initially forms above the centre of the reactor and subsequently a high degree of stratification of the temperature can be seen. It is interesting to compare the horizontal temperature contours seen in case C in Fig. 3, which are most obvious at the centre of the reactor, with the shape of cool flames at terrestrial conditions. Terrestrial cool flames have been described as being horizontal flame fronts with a slight upward curvature in the centre of the reactor, and a slight downward curvature near the walls [8]. This is qualitatively similar to the shape of the temperature contours in Fig. 3. The concentration field is clearly more complex in this case. The top of the reactor is quickly depleted of A. This zone of depletion spreads down the walls of the vessel due to the toroidal flow pattern which develops due to natural convection. Near the bottom of the reactor, there is a small region around the vertical axis which is rich in A due to the lower temperatures in this part of the vessel. Some small-scale oscillations in the temperature and the concentration of A can be seen for case C in Fig. 3; however, it is difficult to discern their exact nature due to their relatively small scale. It is also interesting to look at the temperature distribution at $t = 2.8$ s. Consider the temperature along the horizontal axis of the reactor, moving out from the centre. Near the vertical axis, the temperature is at a maximum, then upon increasing the radius, the temperature of the gas drops. When the radius is increased further the temperature once again increases, before decreasing to the wall temperature in the boundary layer. This variation in temperature is clearly due to the flow patterns in the reactor. The cooler regions, about halfway between the vertical axis and the wall, correspond to the areas of the reactor where the ‘eye’ of the toroidal vortex would be found. The region of higher

temperature near the wall is probably due to the influence of the hotter gas flowing downwards near the wall.

When $\tau_{step\ 2} / \tau_{convection}$ is increased beyond ~ 15, a new region of behaviour is observed, which exhibits more well-defined oscillations. This region is typified by case D in Figs. 2 and 3. The temperature fields seen in Fig. 3 for case D are similar to those seen in case C. The high temperature region is more confined to the top of the reactor. This is, of course, due to the more intense natural convection. At first glance, the oscillations in the temperature and the concentration of A are confined to the hot region in the top half of the reactor. In the much cooler lower half of the reactor, the variations in temperature and concentration are much smaller in magnitude. The smaller hot zone allows the region rich in A around the vertical axis to move further up the reactor than in case C.

When the system moves towards the upper boundary between oscillatory and non-oscillatory behaviour, the oscillations observed become much more heavily damped. They do, however, remain qualitatively similar to those seen in case D. Eventually, the system moves into a region of parameter space where no oscillations occur. In this region, the solutions are similar to case E in Figs. 2 and 3. The concentration of A remains virtually spatially uniform throughout; there is only a very slight decrease in the concentration near the top of the reactor for $t > 5$ s. In this regard, case E is very similar to the low temperature rise solutions with $Ra < 10^3$. The temperature distributions do differ however. The influence of natural convection is clear in case E in Fig. 3. The hot zone initially forms well above the centre of the reactor and a high degree of stratification in the temperature develops.

The pictures of the temperature and concentration fields in Fig 3 allow some qualitative comparison of the behaviour in different regions. The salient differences are more easily seen by examining first the temporal development of the temperature and the concentration of A at the centre of the reactor for each of the cases A – E, and then the spatial development as the reaction proceeds. These comparisons are made, in turn, below.

5.2 Temporal Development of the Temperature and Concentration of A at the Centre of the Reactor

The temporal development of the five cases A – E is shown in Fig. 4. Case A, shown in Fig. 4(a), is typical of the region of sustained oscillations, which is found approximately when $1.5 < \tau_{step\ 2} / \tau_{diffusion} < 1$. This region of sustained oscillations is very similar to that seen in the purely diffusive case [24].

Case B is located in a part of the regime diagram where natural convection should be significant ($Ra \sim 10^4$). Despite this, the temporal development of the temperature and the concentration of A at the centre of the reactor (Fig. 4(b)) are remarkably similar in shape to what they would be in the purely diffusive case. The reason for this was discussed above. Over the first 3 s of the reaction, the temperature and concentration profiles in Fig. 3 show approximate radial symmetry. This is because the temperature rise in the vessel is insufficient to generate natural convection. Indeed, natural convection only becomes significant after ~ 3 s. At this time, however, the concentration of A has risen to its peak and then subsequently fallen back to almost zero.

The first oscillatory case considered in which natural convection is important is case C, shown in Fig. 4(c). The oscillatory behaviour is evidently more complex, and there is a notable difference between this and the behaviour seen in the purely diffusive case. The temporal development of the temperature and the concentration of A, shown in Fig. 4(c), is unlike anything presented previously. The temperature increases rapidly initially, reaching its peak after ~ 2.5 s. The temperature rise is large (~ 95 K) as would be expected given the proximity of this region to the non-oscillatory, high temperature rise solutions in the regime diagram. Whilst the temperature increases, the concentration of A first increases, and then decreases rapidly. So far, this behaviour is similar to what has been observed previously. However, after reaching the peak temperature, the system begins to cool, and the concentration increases, until at ~ 3 s the temperature goes through an inflexion, before continuing downwards. At the same time there is a very small-scale oscillation in the concentration of A, which then continues increasing. After this time, the temperature falls, before increasing very slightly at ~ 5.5 s, then resumes a steady decline. The behaviour exhibited in this case is typical of the solutions in this part

of the regime diagram. These all exhibit very small oscillations in temperature over a long timescale, but also show shorter timescale effects, such as the inflexion in temperature. These effects often take the form of an inflexion in the temperature curve, or there is a small-scale oscillation in the temperature before it either keeps increasing or decreasing. Similar effects to this can be seen in the thermocouple traces in the experimental work on the thermal decomposition of azomethane in the presence of natural convection [31]. Also, small scale oscillations in the temperature at the centre of a spherical vessel have also been observed even in the absence of reaction [32]. Experiments were performed wherein an inert gas was admitted to a preheated vessel. The gas would then heat up to the wall temperature. It was shown that when *Ra* rose above ~ 10^4, the temperature measured at the centre of a spherical vessel would exhibit small-scale oscillations as it approached the wall temperature. The fact that these small-scale inflexions or oscillations occur in the experimental measurement of a non-oscillatory decomposition reaction, and indeed in chemically inert systems, suggests that these small-scale oscillations are due to the fluid mechanics, rather than the oscillatory nature of the reaction. It is interesting to compare the period of the small-scale oscillation in the concentration of A seen at $t \sim 3$ s in Fig. 4(c), with the magnitude of $\tau_{convection}$. For case C, $\tau_{convection} \sim 0.3$ s, which is very similar in magnitude to the period of the oscillation in the concentration.

Case D was shown in Fig. 3 to exhibit anti-phase oscillations in the top half of the reactor; however, no discernible oscillations could be seen lower down the reactor. It is noticeable in Fig. 3(d) that the temperatures measured at the centre of the reactor are significantly lower in case D, than those seen in case C, and in the diffusive limit. It is also evident that there are indeed oscillations in the temperature and the concentration of A. The oscillations have a much smaller amplitude than those seen in the diffusive limit. These smaller amplitude oscillations are typical of those seen at the centre of the region of oscillations defined in Fig. 2. What is perhaps most surprising about case D is that the temperature and concentration are oscillating in-phase at the centre of the reactor. This effect has been described previously [23].

The final case, E, shown in Fig. 4(e) is non-oscillatory and the temporal development of the temperature and the concentration of A are similar to those in the

non-oscillatory, low temperature rise region in the purely diffusive case. In both cases there is a slow growth and decay of both temperature and concentration, and the maximum temperature rise is very small (~ 12 K). Where the two cases do differ, of course, is in the spatial structure.

It is interesting to note that natural convection appears to have very little effect on the temporal development of the temperature and concentration in the reactor in the regions of the regime diagram in which the reaction is non-oscillatory (cases B and E). However, natural convection does play a significant role in the oscillatory solutions (cases A, C and D), where the behaviour can be complex. The complexities introduced by natural convection will be further discussed below when the spatial development of the temperature and the concentration of A in the reactor is considered in greater detail.

5.3 Spatial Development of the Temperature and the Concentration of A

The five cases considered above show a variety of different forms in the temporal development of the temperature and the concentration of A. In addition to this, Fig. 3 also shows that there are considerable differences in the spatial structure of the temperature and concentration fields. To highlight these differences, temperature and concentration profiles along the vertical and horizontal axes are presented, as time progresses, for each of the cases A – E.

5.3.1 Case A

Case A is in the region of sustained oscillations when diffusion dominates transport. Fig. 5 shows the variation along the vertical axis of the reactor of (a) the temperature and (b) the concentration of A. In addition the variation along the horizontal axis of the temperature is shown in Fig. 5(c) and the variation of the concentration of A along the horizontal axis appears in Fig. 5(d). It can be seen from the vertical profile that the initial development of the temperature profile for the first 2 s is approximately symmetric, before it skews slightly at larger times. It is also interesting to see that there is clearly variation in the position of the maximum temperature at different times in the oscillatory

cycle. For example, when the temperature reaches its first maximum at $t \sim 3$ s, the maximum temperature is found at $y = 0.06$ m, whereas at the first trough in the temperature, the maximum is found lower down the reactor at $y = 0.055$ m. The concentration is initially spatially uniform; however, as the temperature in the hot zone of the reactor increases, the rate of depletion of A in this part of the reactor also increases. Between 2 and 3 s, the concentration of A in the top half of the reactor falls from its highest value to almost zero very rapidly. It can also be seen that in the next oscillatory cycle, the concentration rises to very close to its initial maximum value, and is very nearly spatially uniform. As was the case with the location of the maximum temperature, the location of the minimum concentration of A can also be seen to shift up and down as time progresses. For example, at the first trough in concentration at $t = 3$ s (corresponding to the first peak in the temperature), the minimum concentration of A is found at $y = 0.065$ m, whereas at the next peak in the concentration at $t = 6$ s, the minimum concentration is found much closer to the centre of the reactor at $y = 0.055$ m. Finally, it is also interesting to note from Fig. 5(b) that the concentration of A at the bottom of the reactor is significantly higher than that at the top for a large part of the time period considered. This is, of course, due to the weak natural convection skewing the temperature field.

The horizontal temperature profiles are very similar to those seen previously in the purely diffusive regime. The concentration profiles show that the system is oscillating between a case where the concentration is virtually spatially uniform, with the concentration of A at the centre of the reactor being only marginally smaller than that at the wall and a case where the concentration near the centre of the reactor is near zero, whilst the concentration at the wall is significantly higher. This is exactly the same behaviour as was seen for the cases with sustained oscillations in the purely diffusive limit [24].

5.3.2 Case B

Case B is the first case considered in which natural convection plays a significant role. The maximum value of Ra is $\sim 10^4$, which is well into the region in which laminar natural convection is significant. Case B is in a region of the regime diagram close to the

non-oscillatory, high temperature rise regime in the diffusive limit. The vertical profiles of temperature and concentration of A are shown in Fig. 6(a) and (b) and the horizontal profiles in Fig. 6(c) and (d). It was noted above that over the first 2 – 3 s of the reaction, the temperature and concentration fields were approximately symmetric. This is confirmed in Fig. 6. The vertical temperature profiles over the first 3 s in Fig. 6(a) are virtually symmetrical. The shapes of the temperature distributions are also very interesting. There is a large region in the centre of the reactor where the temperature is increasing virtually uniformly. This can be seen in both Fig. 6(a) for the vertical profile and Fig. 6(c) for the horizontal profile. There is therefore a region of constant temperature around the centre of the reactor with a narrow boundary layer near the wall. The shapes of these temperature profiles at small times are virtually identical to those seen in the non-oscillatory, high temperature rise case in the diffusive limit [24]. The development of the concentration profiles are also very similar to what is seen in the purely diffusive limit. The concentration is approximately spatially uniform as it increases initially, but then it very rapidly drops to virtually zero in the bulk of the vessel, with the only significant amounts of A being found in the cooler boundary layer near the wall.

When t increases beyond ~ 3 s, the effects of natural convection are evident. In the vertical temperature profile in Fig. 6(a) the symmetry that was seen for small times is lost and the temperature profile becomes highly skewed, with the highest temperature occurring very close to the top of the reactor. The effects of convection can also be seen in Fig. 6(c). The concentration in the boundary layer at the top of the reactor drops as time progresses, but at the bottom, the concentration in the boundary layer increases. This is due to the skewing of the temperature profile, with the intermediate A being depleted in the hotter top section of the reactor, and accumulating in the cooler bottom section of the reactor. The effects of natural convection can also be seen in the horizontal temperature profile in Fig. 6(c), although these effects are far more subtle than those seen in the vertical profile. Initially, the temperature is constant over a large part of the horizontal axis of the reactor, as described previously. At t = 4 s, when natural convection is just starting to take effect, the temperature profile shows much more curvature, *i.e.* there is no region of uniform temperature around the centre of the reactor. For greater t,

natural convection is significant and the maximum temperature on the horizontal axis decreases slightly. What is interesting is that the temperature is once again virtually constant along a significant fraction of the horizontal axis. The temperature distribution when natural convection becomes significant is therefore dependent on the vertical position, but does not vary significantly with horizontal position. The emergence of this vertical stratification in the temperature is a classic feature of a system in which natural convection is significant, but not extreme.

It was discussed above that natural convection only becomes significant after ~ 3 s. This is more clearly demonstrated if an estimate of the magnitude of the convective term in Eq. (2), describing the conservation of energy, at the centre of the reactor is examined. This appears in Fig. 7. Over the first 3 s of the reaction, the convection term is virtually zero. After 3 s, there is a very large increase in the magnitude of the term as natural convection becomes important. The fact that natural convection does not develop is probably due to the shape of the temperature profile, shown in Fig. 6(a). Initially, the temperature is virtually uniform over the bulk of the vessel, so the temperature gradients, which cause natural convection, are too small to cause significant motion of the gas. The fact that the temperature rise in much of the reactor is uniform suggests that the generation term in Eq. (2) is dominant initially, with the convection term only becoming significant at larger times. This induction time for natural convection is obviously an important property in these systems, and will be discussed further below.

5.3.3 Case C

Case C showed some interesting behaviour in Fig. 4(d), with small scale oscillations in the concentration of A at the centre of the reactor and an inflexion in the temperature curve. The vertical temperature and concentration profiles are shown in Fig. 8(a) and (b). In contrast to case B, it is clear from Fig. 8(a) that natural convection becomes significant at a much lower value of t. A skewed temperature profile quickly develops with the maximum temperature in the top half of the vessel. It is curious to note that at $t = 2.5$ s, which is when the temperature reaches a maximum, the peak in the vertical temperature profile broadens significantly. This is different from any of the conditions considered previously and is somewhat similar in appearance to a flame front

propagating downwards in the vessel (at ~ 8 cm s^{-1}). This peak broadening is short lived, and as the gas cools, the temperature profile more closely resembles the skewed profiles seen previously.

Inspection of Fig. 8(b) for the vertical concentration profile shows that there are two distinct regions in the reactor. There is the relatively cool region at the bottom of the reactor, which is rich in the intermediate A, and then there is the hot zone at the top of the reactor where the concentration of A is virtually zero. The peak broadening effect is also evident; at t = 2.5 s, it can be seen that the region in which the concentration of A in the reactor is close to zero extends much further down the reactor than at any other time. It is this broadening of the temperature peak which causes the unusual shape of the temperature *versus* time curve in Fig. 4(d). The time at which the broadening of the temperature peak in Fig. 8(a) occurs is the same as the time when the maximum temperature is reached in Fig. 4(d). The expansion of the temperature peak in Fig. 8(a) begins at ~ 2 s; this corresponds to the first inflexion in the temperature curve in Fig. 4(d), which can be seen at this time. The temperature profile returns to the more familiar skewed form after ~ 3 s, which corresponds to the second, more obvious inflexion in the temperature curve.

The forms of the horizontal temperature and concentration profiles are also very interesting. These are shown in Fig. 8(c) and (d). It can clearly be seen from Fig. 8(c) that there is very little variation in the temperature over about 70% of the horizontal axis. There is generally a very slight decrease in temperature, moving out from the centre of the reactor initially. The temperature then increases slightly, before falling to the wall temperature in the boundary layer. The maximum in the horizontal temperature profile is due to the flow patterns within the reactor. The temperature is higher due to the hotter gas flowing downwards from the top half of the reactor. The widening of the temperature peak can once again be identified in Fig. 8(c) at 2.5 s, where the temperature at the centre of the reactor shows a very large increase from that at 2 s, whilst the rest of the gas along the horizontal axis heats up considerably less.

The shapes of the concentration profiles along the horizontal axis in Fig. 8(d) are markedly different from anything seen previously. As usual, the concentration increases uniformly along the horizontal axis initially, but as the reaction proceeds, the

concentration profile changes shape. A minimum develops in the concentration profile. This is again due to the influence of the hot gas descending from the top half of the reactor, which has been depleted of A. Eventually, the horizontal profile develops such that the highest concentration of A is at the centre of the reactor, and the concentration falls as the distance from the vertical axis is increased. This concentration profile is in stark contrast to those seen previously, particularly in the diffusive limit, where the concentration is always lowest at the centre of the reactor and increases on moving toward the wall [17, 18, 24].

5.3.4 Case D

Figure 4(a) showed that case D exhibited small scale, in-phase oscillations in the temperature and the concentration of A at the centre of the reactor. Fig. 9(a) and (b) shows the development of the vertical temperature and concentration profiles. The temperature profile is highly skewed, but does not show any of the peak broadening seen in case C. It is interesting to note that the region of the reactor in which the concentration of A is depleted is confined to a very small region near the top of the reactor. In fact, there is very little variation of the concentration of A over the bottom three quarters of the vertical axis. It is also interesting to compare the extent to which the intermediate A is depleted in the hot zone of the reactor with what was seen in Fig. 8 for case C. Despite both cases having similar rises in temperature in the hot zone, case D shows a much smaller drop in the concentration of A in this part of the reactor. This is most likely due to the increased intensity of convection supplying A more efficiently to the hot zone in the reactor. Finally, the large scale anti-phase oscillations in the concentration and temperature can clearly be identified at the top of the reactor, and there is also some evidence of the smaller scale, in-phase oscillations further down the reactor.

The horizontal temperature and concentration profiles, shown in Fig. 9(c) and (d), are very similar in form to those seen for case C, with the temperature being approximately constant over half the radius. As with case C, the temperature then increases due to the influence of the descending hot gas, before decreasing in the boundary layer to the wall temperature. The concentration profiles show that the concentration is highest at the centre of the reactor and decreases on moving outwards

toward the wall. At some times there is a minimum in the concentration profile, close to, but not at, the wall. Once again this is due to the influence of the descending hot gas near the wall of the reactor.

5.3.5 Case E

Case E is in a region of the regime diagram in which no oscillations are observed. In fact, it can be seen from Fig. 4 that the temporal development of the temperature and the concentration of A are very similar to those in the non-oscillatory, low temperature rise regime in the purely diffusive limit [24]. Figure 10(a), which shows the temperature profile along the vertical axis of the reactor for case E, indicates that despite having similar evolution of the temperature at the centre of the reactor to that in the purely diffusive limit, the spatial forms of the solutions are quite different, due entirely of course to the presence of significant natural convection in the former case. In case E the temperature profile is highly skewed, whereas in the purely diffusive case, the profile is approximately symmetric. Despite the difference in the temperature profiles, Fig. 10(b), showing the variation of the concentration of A along the vertical axis, shows that the concentration profiles are virtually uniform, *i.e.* very similar to those seen in the purely diffusive limit. Of course, for case E, the concentration at the top of the reactor is slightly less than at the bottom, due to the skewed temperature profile, but the variation is minimal.

Figure 10(c) and (d) shows the profiles of the temperature and the concentration of A along the horizontal axis for case E. The shape of the temperature profiles is very similar to those in cases C and D. Again, it is clear that there is very little spatial variation in the concentration of A, but it is worth pointing out that the concentration is highest at the centre of the reactor and then decreases towards the wall. This is the opposite of what was seen in the diffusive limit, where the concentration was always at its lowest at the centre of the reactor.

5.3.6 Position of the Maximum Temperature for Cases A – E

It has been shown previously [25, 31] that the position of the maximum temperature on the vertical axis of the reactor varies with Rayleigh number. It is interesting to

compare the variation of the position of the maximum temperature derived experimentally [31], and numerically [25], for the thermal decomposition of azomethane, with the results for Sal'nikov's reaction, described above. Figure 11 shows the best fit line through the measured and simulated points, giving the variation of the position of the maximum temperature along the vertical axis of the reactor, with Rayleigh number, which has been calculated using the temperature rise at the centre of the reactor. Also plotted are points representing cases A – E, discussed above. The simulations for Sal'nikov's reaction agree very well with the results, both experimental and numerical, for the decomposition of azomethane.

5.4 Induction Times for Natural Convection

It was noted above that for case C, the system developed for ~ 3 s before natural convection became significant. This induction time for natural convection is clearly very important. It is especially important for explosive systems, because it is possible that a system could explode before natural convection has had a chance to develop to cool the system. Merzhanov and Shtessel [33] compared the induction time for explosion with an expression for the induction time for convection:

$$\tau_i = 70 Ra^{-2/3} Pr^{5/6} . \qquad (11)$$

It should be noted that this expression was developed through the study of natural convection in a plane layer of inert fluid, heated from below. It is not clear whether this expression was derived theoretically or empirically. Equation (11) suggests that the induction time for natural convection is only a function of the Rayleigh number, with higher *Ra* having lower induction times. A cursory inspection of the numerical results used in the production of Fig. 2 suggests that this is not the case for this system, which includes chemical reaction. It is sensible to assume that the kinetics of the reaction would also play a role in determining the induction time for natural convection. The form of the expression for the induction time when reaction is important has, however, not been considered further in this work.

It is interesting to note, however that the effects of natural convection 'switching on' are evident in both the temporal and spatial developments of the cases considered above. The disruption of the spherical symmetry expected in the absence of natural convection is clear from Fig. 3 and from the vertical temperature profiles in Figs. 6, 8, 9 and 10. There is also evidence for the onset of natural convection in the temporal development of the temperature at the centre of the reactor for cases C – E in Fig. 4. Inspection of Fig. 7(a) indicates that natural convection becomes important after 1 – 2 s (this is the period when the vertical temperature profile moves from approximately spherically symmetric to highly skewed). At $t \sim 1.5$ s in Fig. 4(c) there is a decrease in the slope of the temperature *versus* time curve. This change is due to the convective term in Eq. (2) becoming important. Similar decreases in gradient in the temperature *v.* time curves for cases D and E are also evident in Fig. 4, after ~ 1.5 s for case D and after ~ 1 s for case E. Inspection of Figs. 9(a) and 10(a) shows that these times correspond to the approximate transition to a highly skewed vertical temperature profile.

6. Conclusions

The behaviour of Sal'nikov's reaction has been examined under the influence of natural convection to determine the region on the regime diagram, for fixed $\tau_{step\ 2} / \tau_{step\ 1}$, in which oscillations occur. The region found could be split into two distinct areas, one for $Ra < 10^3$, where diffusion dominates transport, and one when $10^3 < Ra < 10^6$, when laminar convection dominates. There was a very noticeable change in shape of the region of oscillations around the critical value of $Ra \sim 10^3$, when natural convection supercedes diffusion as the principal means of heat and mass transport. As one might have anticipated, when diffusion dominated transport, the boundaries between oscillatory and non-oscillatory solutions are largely independent of $\tau_{step\ 2} / \tau_{convection}$, and agreed well with the values found previously in the purely diffusive limit. When natural convection was important, the oscillations occurred over a wider range of parameters, and the width of the oscillatory region increased with Ra.

In addition to defining a region of oscillations, the different types of behaviour in different parts of the regime diagram were discussed. In general, it was observed that the inclusion of natural convection led to a number of different types of behaviour. In most cases the spatial temperature and concentration fields were far more complex than those seen in the absence of natural convection. Specifically, it was shown that for the non-oscillatory cases with relatively small increases in temperature, the temporal evolution of the temperature and the concentration of A at the centre of the reactor was similar, regardless of the degree of convection present. In addition, it was shown that in this region of slow reaction, the concentration of A remained virtually spatially uniform at Rayleigh numbers sufficient to generate significant natural convection. This is similar to the diffusive case. Natural convection did, however, have an impact on the shape of the temperature profile along the vertical axis of the reactor. The profile becomes more skewed as *Ra* is increased. Finally, for the non-oscillatory, high temperature rise solutions with natural convection, the forms of the solutions were found to be initially very similar to those seen in the purely diffusive limit. This is because it takes some time for sufficient temperature gradients to develop to induce significant natural convection.

Acknowledgements

The financial support of the Engineering and Physical Sciences Research Council is gratefully acknowledged. We are also very grateful to Prof. J.F. Griffiths for many very helpful discussions over the course of this work.

References

[1] J.F. Griffiths, J.A. Barnard, Flame and Combustion, 3rd edn, Blackie, Glasgow, 1995, pp. 181–205.

[2] J.H. Knox, in: P.G. Ashmore, F.S. Dainton and T.M. Sugden (Eds.), Photochemistry and Reaction Kinetics, Cambridge University Press, Cambridge, 1967, pp. 250–286.

[3] J.S. Turner, Buoyancy Effects in Fluids, Cambridge University Press, Cambridge, 1979, pp. 207 – 250.
[4] J.F. Griffiths, Prog. Energy Combust. Sci. 21 (1995) 25 – 107.
[5] A. Melvin, Combust. Flame 13 (1969) 438 – 439.
[6] D.C. Bull, D.B. Pye, C.P. Quinn, Combust. Flame 28 (1977) 207 – 211.
[7] H. Pearlman, Combust. Flame 121 (2000) 390 – 393.
[8] M. Foster, H. Pearlman, Combust. Flame 147 (2006) 108 – 117.
[9] H. Pearlman, Combust. Flame 148 (2007) 280 – 284.
[10] I.E. Sal'nikov, Zh. Fiz. Khim. 23 (1949) 258 – 272.
[11] L.K. Forbes, Proc. R. Soc. London A 430 (1990) 641–651.
[12] B.F. Gray, M.J. Roberts, Proc. R. Soc. London A 416 (1988) 391–402.
[13] P. Gray, S.K. Scott, Chemical Oscillations and Instabilities, Clarendon Press, Oxford, 1990, pp. 83 – 111.
[14] P. Gray, S.R. Kay, S.K. Scott, Proc. R. Soc. London A 416 (1988) 321–341.
[15] S.R. Kay, S.K. Scott, Proc. R. Soc. London A 416 (1988) 343–359.
[16] P. Gray, S.K. Scott, Chemical Oscillations and Instabilities, Clarendon Press, Oxford, 1990, pp. 264 – 291.
[17] R. Fairlie, J.F. Griffiths, Faraday Discuss. 120 (2001) 147–164.
[18] R. Fairlie, J.F. Griffiths, Math. Comput. Model. 36 (2002) 245–257.
[19] S.S.S. Cardoso, P.C. Kan, K.K. Savjani, A.N. Hayhurst, J.F. Griffiths, Combust. Flame 136 (2004) 241–245.
[20] S.S.S. Cardoso, P.C. Kan, K.K. Savjani, A.N. Hayhurst, J.F. Griffiths, Phys. Chem. Chem. Phys. 6 (2004) 1687–1696.
[21] A.N. Campbell, S.S.S. Cardoso, A.N. Hayhurst, Proc. R. Soc. London A 461 (2005) 1999 – 2020.
[22] A.N. Campbell, S.S.S. Cardoso, A.N. Hayhurst, Chem. Eng. Res. Des. 84(A7) (2006) 553 – 561.
[23] A.N. Campbell, S.S.S. Cardoso, A.N. Hayhurst, Chem. Eng. Sci. 60 (2005) 5705 – 5717.
[24] A.N. Campbell, S.S.S. Cardoso, A.N. Hayhurst, Phys. Chem. Chem. Phys. 8 (2006) 2866 – 2878.

[25] A.N. Campbell, S.S.S. Cardoso, A.N. Hayhurst, Chem. Eng. Sci. 62 (2007) 3068 – 3082.
[26] B.J. Tyler, Combust. Flame 10 (1966) 90 – 91.
[27] P.G. Ashmore, B.J. Tyler, T.A.B. Wesley, Proc. Combust. Inst. 11 (1967) 1133 – 1140.
[28] CSIRO, 2000. Fastflo Tutorial Guide, (version 3), CSIRO, Australia.
[29] J.F. Griffiths, S.R. Kay, S.K. Scott, Proc. Combust. Inst. 22 (1988) 1597–1607.
[30] P. Gray, J.F. Griffiths, Combust. Flame 78 (1989) 87–98.
[31] W.H. Archer, Heat transfer mechanisms in exothermic reactions, Ph.D. Thesis, University of Manchester Institute of Science and Technology, 1977.
[32] B.J. Tyler, A.F. Tuck, Int. J. Heat Mass Transfer 10 (1967) 251 – 253.
[33] A.G. Merzhanov, E.A. Shtessel, Astronaut. ACTA 18 (1973) 191–199.

Tables

Table 1. Details of cases A – E shown on the regime diagram in Fig. 2.

case	L / m	g / m s^{-2}	$\kappa \times 10^4$ / m^2 s^{-1}	$\tau_{step\ 2}$ / $\tau_{convection}$	$\tau_{step\ 2}$ / $\tau_{diffusion}$
A	0.05	15	7.5	11.75	1.13
B	0.05	0.5	0.5	3.78	0.08
C	0.01	4.9	0.066	13.84	0.25
D	0.01	30	0.097	25.33	0.37
E	0.01	200	0.2	47.68	0.75

Figure Captions

Fig. 1. The general three-dimensional regime diagram describing the system, where the axes represent ratios of the characteristic timescales for reaction diffusion and convection.

Fig. 2. Two-dimensional representation of the regime diagram in Fig. 1, for $\tau_{step\ 2} / \tau_{step\ 1}$ = 0.094. The shaded region shows where oscillations in the temperature and concentration of A occur. Also shown are two lines of constant *Ra*, corresponding to the approximate transition from weak flow to laminar flow ($Ra = 10^3$), and from laminar flow to turbulent flow ($Ra = 10^6$). The points A – E marked on the diagram correspond to the situations discussed in section 5.

Fig. 3. Development of the temperature (top) and concentration of A (bottom) for a vertical cross-section through the centre of the reactor for cases A – E. The progress of the reaction is shown for 8 s for cases A, C, D and E, and for 6.4 s for case B. The frames are separated by 0.4 s.

Fig. 4. Plots showing the temporal development of the temperature and the concentration of the intermediate A at the centre of the reactor, for cases A – E on the regime diagram in Fig. 2. Details of the parameters used in the simulations appear in Table 1. In each case, the temperature is the solid line and the concentration of A is the dashed line.

Fig. 5. (a) Profiles of the temperature along the vertical axis of the reactor for increasing values of time for case A. (b) Profiles of the concentration of A along the vertical axis for case A for increasing time. (c) Profile of the temperature along the horizontal axis of the reactor for increasing time for case A. (d) Profile of the concentration of A along the horizontal axis of the reactor for case A for increasing time.

Fig. 6. (a) Profiles of the temperature along the vertical axis of the reactor for increasing time for case B. (b) Profiles of the concentration of A along the vertical axis for case B for increasing time. (c) Profile of the temperature along the horizontal axis of the reactor

for increasing time for case B. (d) Profile of the concentration of A along the horizontal axis of the reactor for case B for increasing time.

Fig. 7. Development of the convective term in Eq. (2) at the centre of the reactor for case B.

Fig. 8. (a) Profiles of the temperature along the vertical axis of the reactor for increasing values of time for case C. (b) Profiles of the concentration of A along the vertical axis for case C for increasing time. (c) Profile of the temperature along the horizontal axis of the reactor for increasing times for case C. (d) Profile of the concentration of A along the horizontal axis of the reactor for case C for increasing time.

Fig. 9. (a) Profiles of the temperature along the vertical axis of the reactor for increasing time for case D. (b) Profiles of the concentration of A along the vertical axis for case D for increasing time. (c) Profile of the temperature along the horizontal axis of the reactor for increasing time for case D. (d) Profile of the concentration of A along the horizontal axis of the reactor for case D for increasing time.

Fig. 10. (a) Profiles of the temperature along the vertical axis of the reactor for increasing time for case E. (b) Profiles of the concentration of A along the vertical axis for case E for increasing time. (c) Profile of the temperature along the horizontal axis of the reactor for increasing time for case E. (d) Profile of the concentration of A along the horizontal axis of the reactor for case E for increasing time.

Fig. 11. Variation of the dimensionless position of the maximum temperature along the vertical axis of the reactor with *Ra*. The line is the best fit through the simulated points in [25] for the thermal decomposition of azomethane. The diamonds correspond to cases A – E, discussed above.

Figures

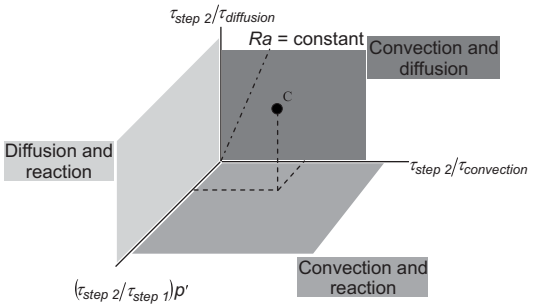

Fig. 1

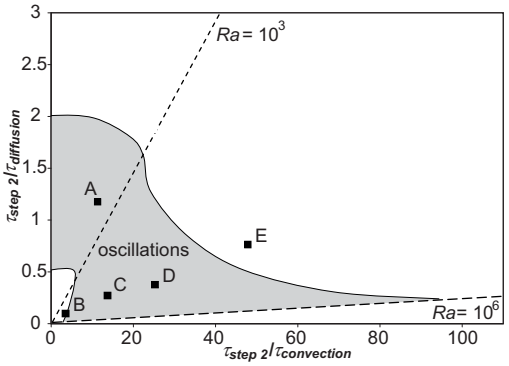

Fig. 2

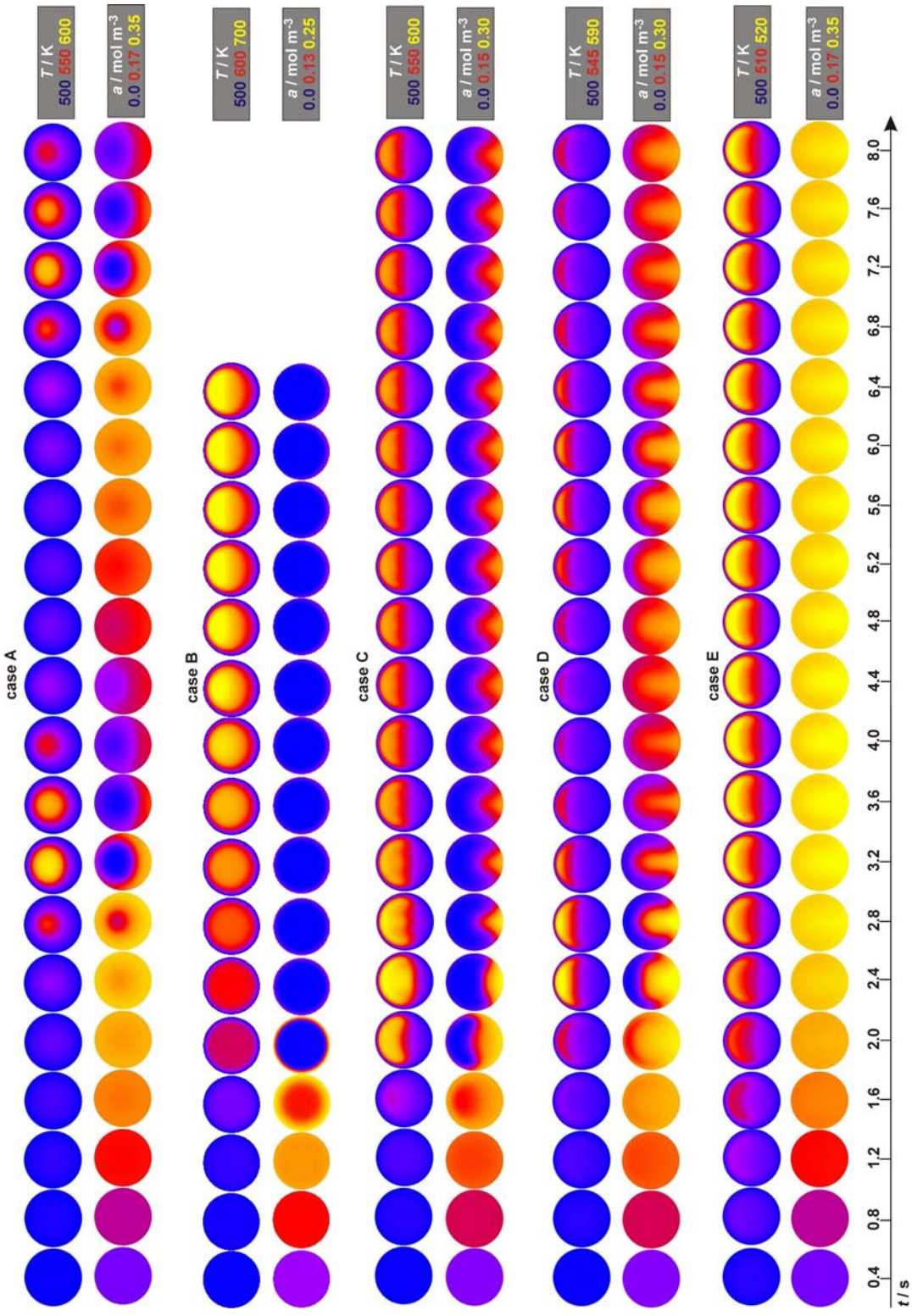
case A
T / K
500 550 600
a / mol m-3
0.0 0.17 0.35
case B
T / K
500 600 700
a / mol m-3
0.0 0.13 0.25
case C
T / K
500 550 600
a / mol m-3
0.0 0.15 0.30
case D
T / K
500 545 590
a / mol m-3
0.0 0.15 0.30
case E
T / K
500 510 520
a / mol m-3
0.0 0.17 0.35
0,4 0,8 1,2 1,6 2,0 2,4 2,8 3,2 3,6 4,0 4,4 4,8 5,2 5,6 6,0 6,4 6,8 7,2 7,6 8,0
t / s

Fig. 3

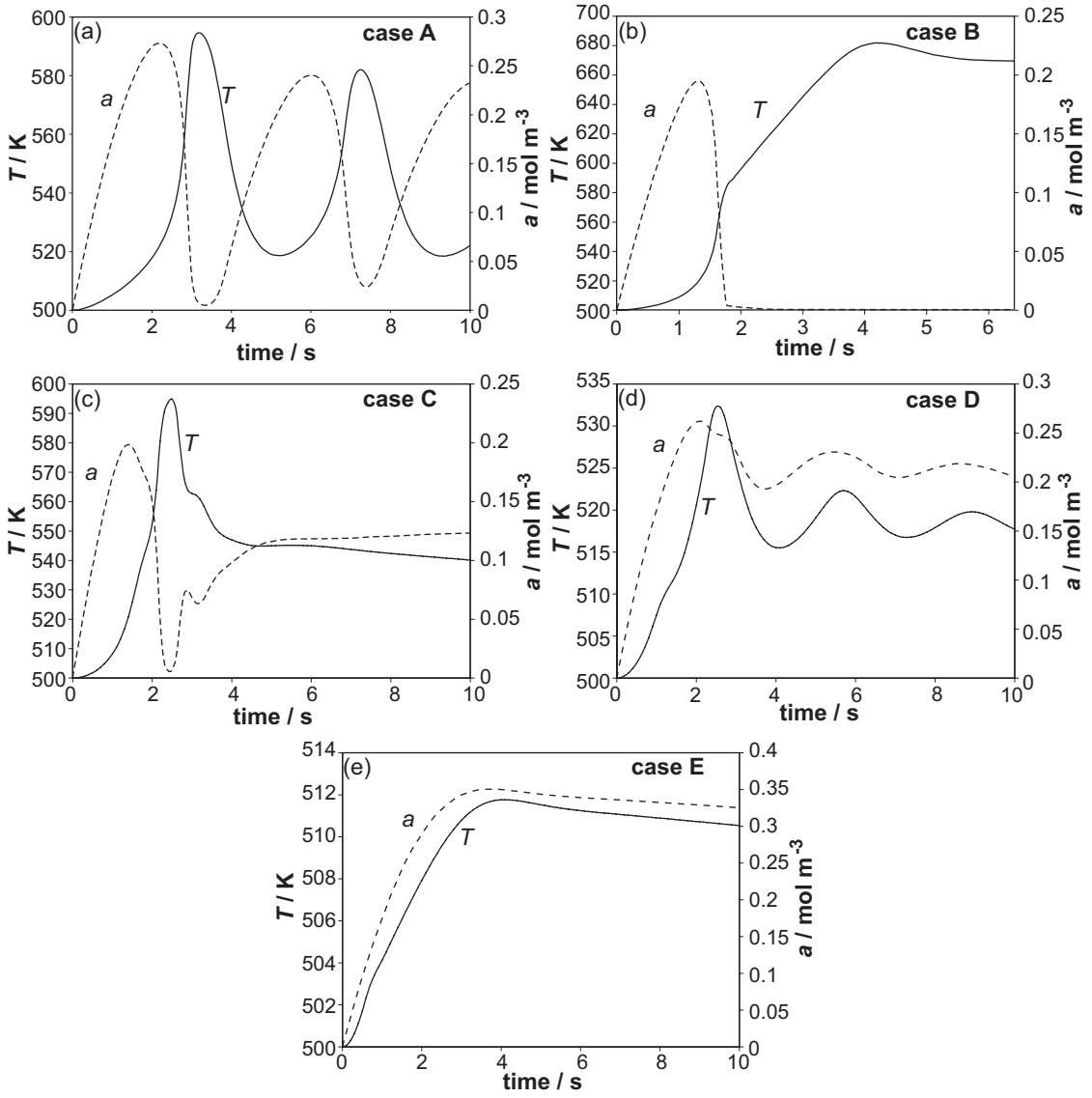

Fig. 4

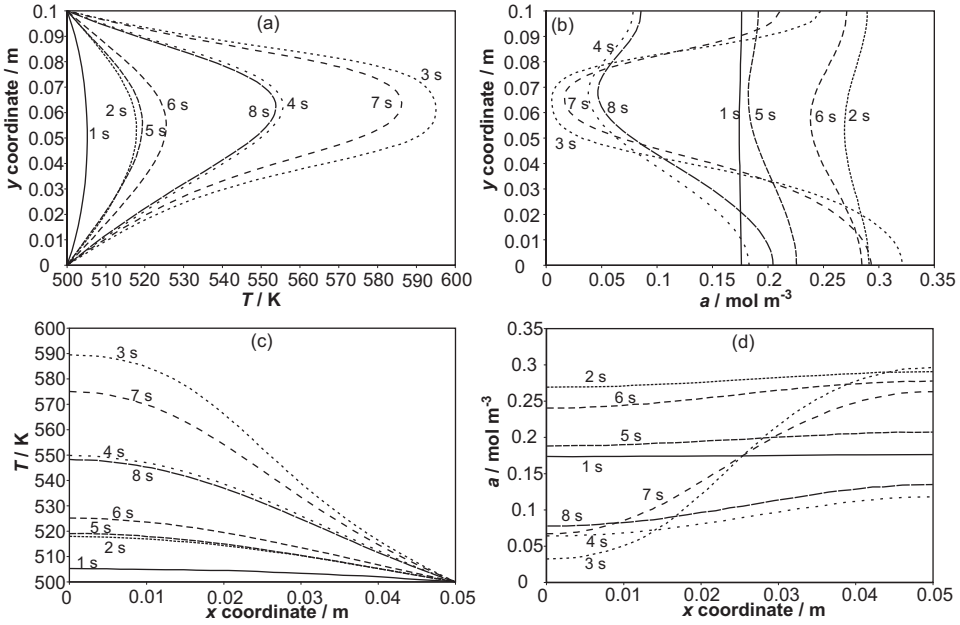
(a)
y coordinate / m
T / K
1 s
2 s
3 s
4 s
5 s
6 s
7 s
8 s
(b)
y coordinate / m
a / mol m-3
(c)
T / K
x coordinate / m
(d)
a / mol m-3
x coordinate / m

Fig. 5

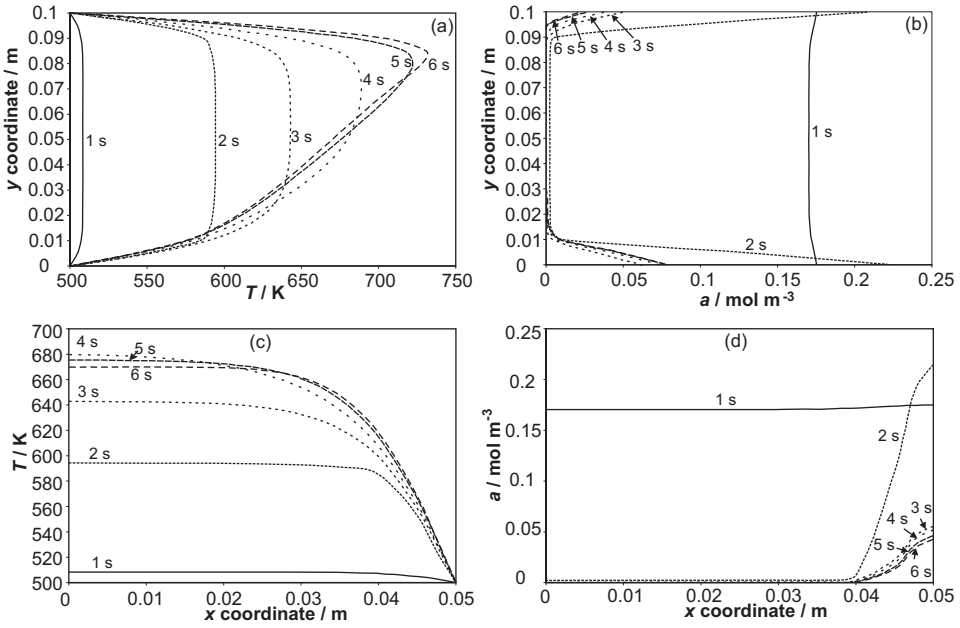
(a)
y coordinate / m
T / K
1 s
2 s
3 s
4 s
5 s
6 s
(b)
y coordinate / m
a / mol m-3
(c)
T / K
x coordinate / m
(d)
a / mol m-3
x coordinate / m

Fig. 6

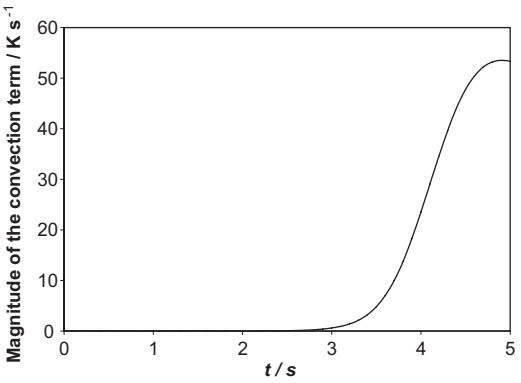
Magnitude of the convection term / K s-1
t / s

Fig. 7

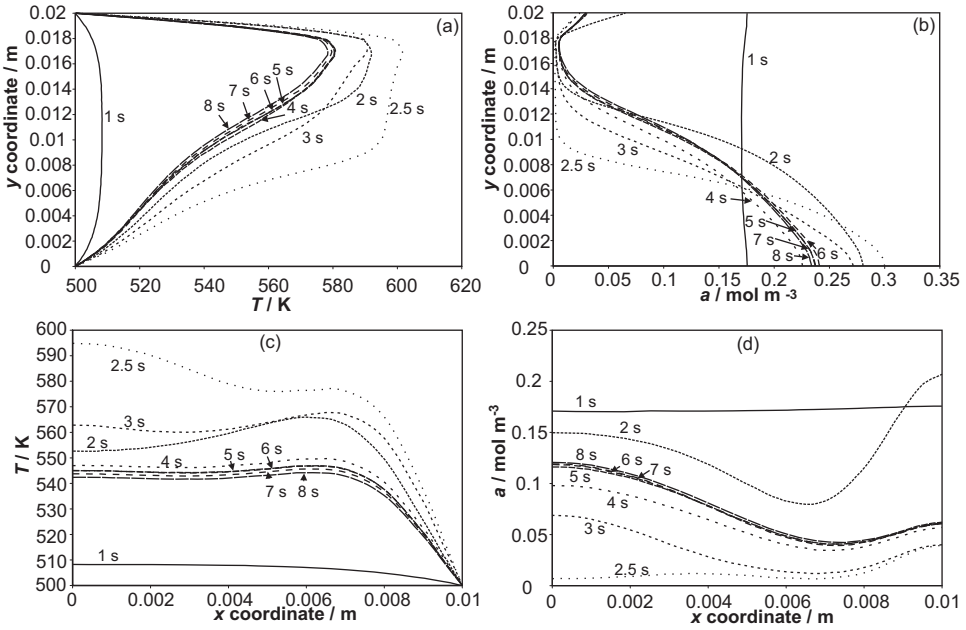
(a)
y coordinate / m
T / K
1 s
2 s
2.5 s
3 s
4 s
5 s
6 s
7 s
8 s
(b)
y coordinate / m
a / mol m -3
(c)
T / K
x coordinate / m
(d)
a / mol m-3
x coordinate / m

Fig. 8

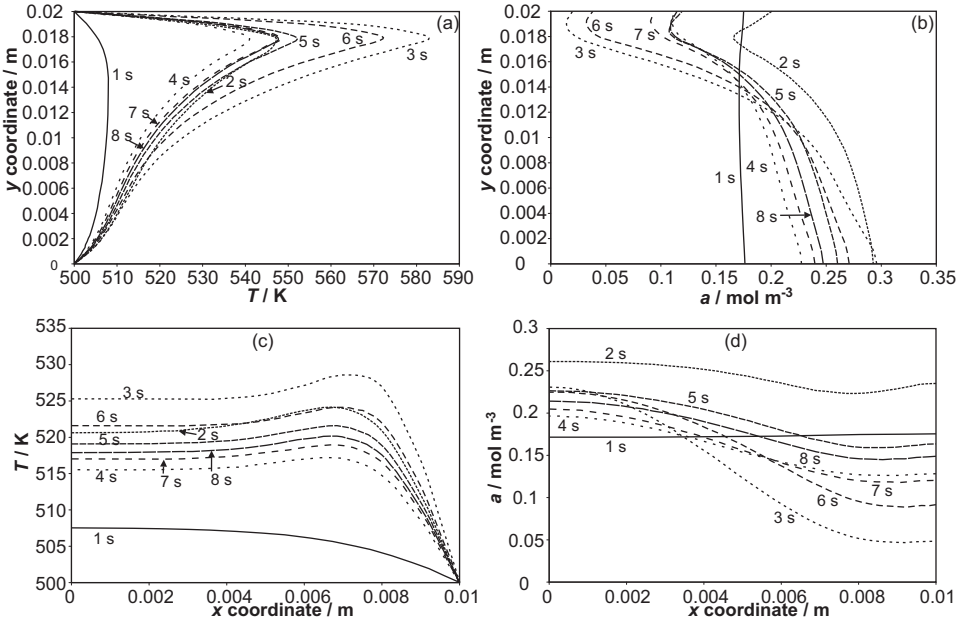
(a)
y coordinate / m
T / K
1 s
2 s
3 s
4 s
5 s
6 s
7 s
8 s
(b)
a / mol m-3
(c)
T / K
x coordinate / m
(d)
a / mol m-3
x coordinate / m

Fig. 9

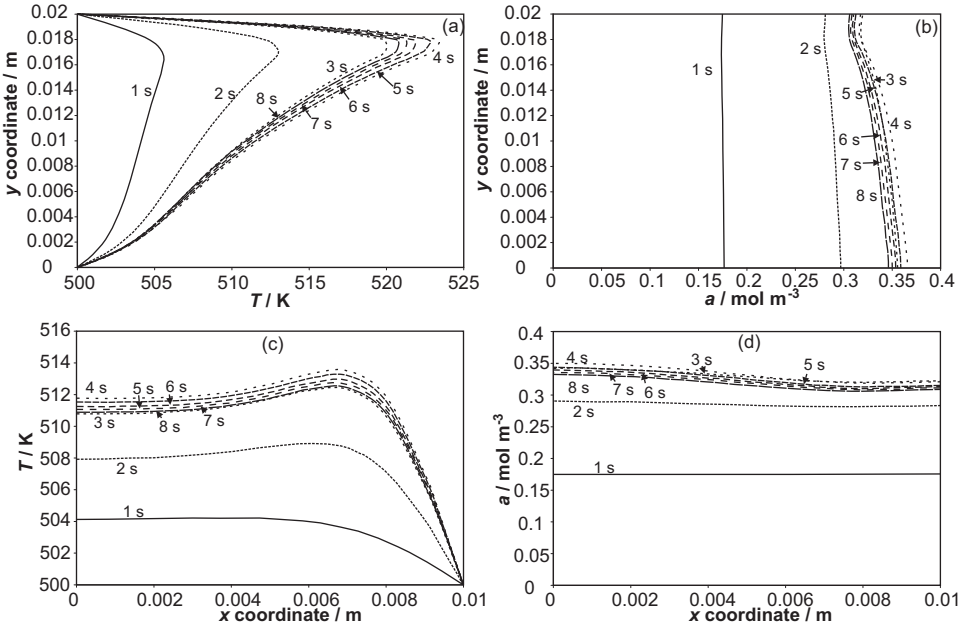
(a)
y coordinate / m
T / K
1 s
2 s
3 s
4 s
5 s
6 s
7 s
8 s
(b)
a / mol m-3
(c)
T / K
x coordinate / m
(d)
a / mol m-3
x coordinate / m

Fig. 10

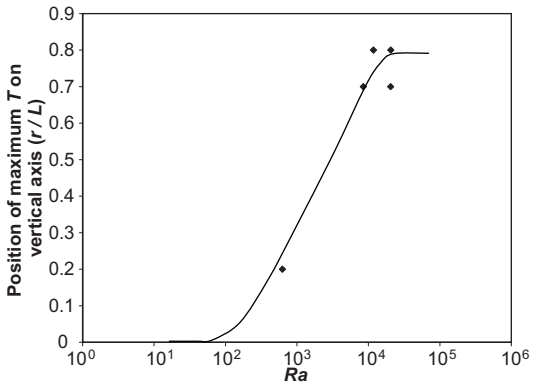
Position of maximum T on vertical axis (r / L)
0.9
0.8
0.7
0.6
0.5
0.4
0.3
0.2
0.1
0
10^0
10^1
10^2
10^3
10^4
10^5
10^6
Ra

Fig. 11